Biosensors and Bioelectronics 124–125 (2019) 115–121

Contents lists available at ScienceDirect

Biosensors and Bioelectronics

journal homepage: www.elsevier.com/locate/bios

Modularization of three-dimensional gold nanoparticles/ferrocene/liposome cluster for electrochemical biosensor

Tingjun Chen[a], Anzhi Sheng[a], Yong Hu[b], Dongsheng Mao[a], Limin Ning[c], Juan Zhang[a,*]

[a] Center for Molecular Recognition and Biosensing, School of Life Sciences, Shanghai University, Shanghai 200444, PR China
[b] State Key Laboratory of Advanced Special Steel, Shanghai University, Shanghai 200444, PR China
[c] College of Medicine and Life Sciences, Nanjing University of Chinese Medicine, Nanjing 210023, PR China

ARTICLE INFO

Keywords:
Three-dimensional gold nanoparticles/ferrocene/liposome cluster
Electrochemical biosensor
Lipopolysaccharide

ABSTRACT

For electrochemical biosensors, just like a computer, the modularization and coordinated operation of different components will facilitate the development of versatile biosensors and effectively reduce costs. However, the efficient synergy between different modules is always difficult. It would be a beneficial way to construct the multi-functional module. In this work, a three-dimensional gold nanoparticles/ferrocene/liposome cluster (GFLC) is fabricated and explored as a building block for the fabrication of an electrochemical biosensor, in which gold nanoparticles, ferrocene and liposome cluster work as a signal amplification component, a signal output component and a molecular recognition component, respectively. With the synergy of multi-functions, GFLC has been successfully applied for electrochemical analysis of lipopolysaccharide (LPS) in food samples. LPS can be linearly assayed in the range from 2×10^{-9} μg/mL to 8 μg/mL with a detection limit of 0.51×10^{-10} μg/mL. In view of the favorable modularization effect, GFLC shows a great potential in the development of electrochemical biosensor with considerable versatility and cost-efficiency.

1. Introduction

Design and fabrication of modularization have become an important part for development of electrochemical biosensors which can be served for on-site, affordable, and rapid point-of-care quantitative analysis (Kumarasamy et al., 2018; Nie et al., 2013). In view of complicated design, expensive labeling, delicate enzyme, or tedious treatments of the existing electrochemical biosensor, it is urgent for us to strive for the electrochemical sensing module to realize a simple "drop-and-measure" assay, which will play a crucial role for medical diagnostics and food safety and risk analysis (Zhang et al., 2013). Thereby a good way is to design multi-functional composites which have the capabilities including molecular recognition, signal output and amplification, so as to meet the demand for the simple electrochemical assay.

Currently, three-dimensional nanocomposites such as three-dimensional porous Pt-Pd nanoparticles supported by graphene–multiwalled carbon nanotube composite (Yuan et al., 2014), three-dimensional Au nanoparticles/nano-poly(3,4-ethylene dioxythiophene)-graphene aerogel nanocomposite (Jia et al., 2018), and three-dimensional graphene-Ag nanoparticles (Chen et al., 2018), have been extensively explored in view of their excellent properties including electrocatalytic activity, fine biocompatibility, and good conductivity. These nanocomposites can well benefit signal amplification, but their relative little function limits the application as an electrochemical module for convenient and easy assay. Consequently, it is favorable to explore the multi-functionality of the three-dimensional cluster as a building block for establishment of electrochemical biosensors.

Nanoliposome can be served as basis for construction of the three-dimensional cluster as a building block. Due to its high specific surface area, the tremendous interface can be provided for the immobilization of nanoparticles which exhibit the property of signal amplification for the fabrication of electrochemical biosensor (Lei and Ju, 2012; Luo et al., 2006; Prakash et al., 2013; Tian and Tetsu, 2005; Wang and Hu, 2009). Meanwhile, the nanoliposome can be easily functionalized through self-assembly of commercial reactive PEG reagents (Bui et al., 2015; Lee et al., 2008; Qian et al., 2016; Sun et al., 2018; Zhang et al., 2017; Zhou et al., 2013), which provides various sites for the linkage of electroactive substances and diverse molecular recognition units for analysis of different targets.

Herein, a universal building block has been designed and constructed through self-assembly of ferrocene (Fc) tagged nanoliposome followed by the integration of gold nanoparticles (AuNPs) to form three dimensional AuNPs/Fc/liposome cluster (GFLC). The GFLC can further serve for sensitive detection of lipopolysaccharide (LPS) which is of a

* Corresponding author.
E-mail address: juanzhang@shu.edu.cn (J. Zhang).

https://doi.org/10.1016/j.bios.2018.09.101
Received 19 July 2018; Received in revised form 18 September 2018; Accepted 30 September 2018
Available online 09 October 2018
0956-5663/

particular interest in medical, therapeutics, and food security because LPS induces microcirculation disturbance, fever reaction, diarrhea, septic shock, and disseminated intravascular coagulation (Beutler and Rietschel, 2003; Murai et al., 1987; Yang et al., 1998). Except for signal amplification and output, GFLC plays a key role in molecular recognition with exposure of hydrazine groups binding with oxidized product of LPS. For electrochemical biosensor, multi-functionalized GFLC will simplify the experimental procedure to meet the demand of the portable, on-site analytical device.

2. Materials and methods

2.1. Materials and reagents

Lipopolysaccharide (LPS) from Pseudomonas aeruginosa 10, galactose oxidase (GalO), alkaline phosphatase (ALP), ovalbumin (Ova), dopamine hydrochloride (DA), adenosine 5′-triphosphate disodium salt hydrate (ATP), N-hydroxysuccinimide (NHS), glyceraldehyde 3-phosphate (GAP), cysteamine (Cys), N, N-Dimethylformamide (DMF), sodium perchlorate, sodium phosphate monobasic dihydrate, sodium phosphate dibasic dehydrate, potassium chloride, potassium hexacyanoferrate(III), and potassium hexacyanoferrate(IV) were purchased from Sigma (Shanghai, China). Pyrene-1-boronic acid (PBA) was obtained from Aladdin (Shanghai, China). Bovine serum albumin (BSA), ferrocenecarboxylic acid, 1-(3-dimethlaminopropyl)-3-ethylcarbodimide hydrochloride (EDC), ethyl alcohol, and chloroform were obtained from Sinopharm Chemical Reagent Co., Ltd (Shanghai, China). The 1,2-Distearoyl-*sn*-glycero-3-phosphoethanolamine (DSPE) conjugated polyethylene Glycol 2000 and hydrazine (DSPE-PEG-Hydrazine) and 1,2-Distearoyl-*sn*-glycero-3-phosphoethanolamine (DSPE) conjugated polyethylene Glycol 2000 and NH_2 (DSPE-PEG-NH_2) were obtained from Peng Sheng Biological Co., Ltd (Shanghai, China). Vybrant® DiO Cell-Labeling solution was obtained from Thermo Fisher Scientific (Shanghai, China). Purified water (Nongfu Spring, Nongfu Spring Incorporated Company, China), full-fat sterilization milk (DELUXI, Inner Mongolia Mengniu Dairy Co. Ltd, China), grapefruit juice (Wei Chuan, Hangzhou Weiquan Food Co. Ltd, China), and green tea (Nongfu Spring, Nongfu Spring Incorporated Company, China) were purchased from Shanghai education supermarket. Other reagents were analytical grade and the deionized water used was purified by using a Millipore Milli-Q water purification system (Barnstead, USA) with a resistance value of 18 MΩ cm.

2.2. Preparation and characterization of three dimensional AuNPs/Fc/liposome cluster (GFLC)

2.2.1. Preparation of GFLC

AuNPs were synthesized according to our previous method (Deng et al., 2014). Typically, 95.5 mL of deionized water was heated to boiling in three neck flask, followed by the addition of 1 mL of chloroauric acid solution (10 mg/mL) with magnetic stirring under heating condition. After 5 min, 3.5 mL trisodium citrate (10 mg/mL) was further mixed. When the color of the solution changes from pale yellow to red wine, the mixture was stopped to heat while stirring was continued for 45 min. Finally, the reaction solution was kept in the dark for 12 h and then cooled to room temperature. After centrifugation, the AuNPs were obtained and stored in a brown bottle at 4 °C.

For modification of AuNPs, 200 μL Cys aqueous solution (38.5 μM) was mixed with 40 mL AuNPs solution with stirring overnight at 25 °C to give the Cys modified AuNPs (AuNPs-Cys). Then 400 μL GAP aqueous solution (191 μM) was mixed with 40 mL AuNPs-Cys for 3 h to give GAP modified AuNPs (AuNPs-Cys-GAP) with formation of phosphoramidate bond. After centrifugation, AuNPs-Cys-GAP were dispersed in 0.01 M $NaClO_4$ (pH = 7.0).

For preparation of ferrocene tagged liposome (FTL), DSPE-PEG-NH_2 was firstly reacted with ferrocenecarboxylic acid to give DSPE-PEG-Ferrocene (DSPE-PEG-Fc) (see Supporting information). Subsequently, DSPE-PEG-Fc and DSPE-PEG-hydrazine were dissolved in chloroform at a concentration ratio of 1: 1, followed by drying with nitrogen to give a thin film. The film was resuspended in 2 mL $NaClO_4$ (0.01 M, pH = 7.0) and then sonicated for 45 min to obtain FTL. Finally, 40 mL AuNPs-Cys-GAP was mixed with 400 μL FTL for 30 min to give the three dimensional AuNPs/Fc/liposome cluster (GFLC).

2.2.2. Characterization of GFLC

2.2.2.1. Atomic force microscopy (AFM). 10 μL FTL, GFLC, and AuNPs-Cys-GAP were separately dropped onto freshly-cleaved sheets of mica. After drying in a desiccator overnight, the samples were imaged by using atomic force microscopy (Agilent 5500, Agilent Technologies Co Ltd, USA) at a scan rate of 325 kHz in tapping mode. The images were acquired at a resolution of 512 × 512 pixels. AFM tips (NSC15/AI BS, MikroMasch, Estonia) with force constant in the range 40 N/m were used.

2.2.2.2. Scanning electron microscopy (SEM). AuNPs-Cys-GAP, FTL, and GFLC were separately dropped onto a copper mesh (300 mesh) covered with a carbon membrane and subsequently dried at the room temperature. The samples were characterized by using scanning electron microscopy (Nova NanoSEM 450, Field Electron and Ion Company, USA).

2.2.2.3. Fluorescence spectroscopy. FTL and GFLC were washed and stained with 5 μM Dio. By using fluorescence spectroscopy (F-7000, Hitachi, Ltd., Japan), the fluorescence spectra were measured in the range from 500 nm to 650 nm with 484 nm of excitation wavelength.

2.2.2.4. Confocal laser fluorescence imaging. After staining with Dio for 15 min, FTL and GFLC were separately dropped onto glass slides for imaging by the laser scanning confocal fluorescence microscope (FV3000, Olympus, Japan).

2.2.2.5. Fourier transforms infrared (FT-IR) spectroscopy. The FT-IR spectra were measured by the VERTEX 70 Fourier transform infrared spectroscopy instrument with the deuterium triglycine sulfate detector. The spectrometric measurements were performed at room temperature with a resolution of 0.2 cm^{-1} in the range of 4000 cm^{-1} to 400 cm^{-1}, and the OPUS/IR analysis software was used to calibrate all the scanning spectra.

2.3. Modification of graphite electrode

The graphite electrode (GE) was consecutively polished with 3000 mesh and 5000 mesh sandpaper and 0.05 μM alumina powder. After that, the electrodes were ultrasonically cleaned in ethanol and water for 3 min, respectively, and then dried with nitrogen. Subsequently, the treated electrode was immersed in DMF containing 10 mM PBA for 2 h at room temperature, followed by rinsing with DMF and deionized water, to give PBA modified GE, PBA/GE.

2.4. LPS assay

75 μL LPS in 10 mM PBS buffer (pH = 6.0) with different concentrations were incubated with 5 μL GalO (160 mU/mL) at 25 °C for 10 min. Subsequently, the PBA/GE was immersed in the reacting solution for 30 min to give LPS/PBA/GE. After ordinally washing with 10 mM PBS (pH = 6.0) and deionized water, the modified electrodes were further immersed in 80 μL GFLC for 1 h. The modified electrodes were consecutively rinsed with 0.01 M $NaClO_4$ and deionized water to obtain GFLC/LPS/PBA/GE used for electrochemical detection.

2.5. Specificity analysis and recovery experiment

We studied the specificity of the method with the probably interfering substances including BSA, Ova, ALP, DA, and ATP instead of LPS. In addition, we further investigate anti-interfering ability of the method through adding LPS at different concentrations into soft drinks samples. LPS concentrations were determined by using the established method and recovery ratios were calculated.

2.6. Electrochemical measurement

The cyclic voltammetry (CV) and differential pulse voltammetry (DPV) measurements were performed on a CHI660C electrochemical workstation (CH Instruments, Shanghai, China) using a three electrode cell. The modified electrode was used as working electrode with saturated calomel electrode (SCE) as reference electrode and platinum wire electrode as counter electrode. CV was performed over the potential range from 0 V to 0.8 V at a scan rate of 100 mV/s using 0.01 M $NaClO_4$ (pH = 7.0). The DPV was measured in the range from 0.2 V to 0.6 V with 50 mV of amplitude and 50 ms of pulse width.

2.7. Statistical analysis

All determinations were triplicates, and mean values as well as standard deviations were calculated. Analysis of variance (ANOVA) was performed and the mean separation was done by LSD ($p \leq 0.05$) using SPSS 13.0 program for windows (SPSS Inc., IL, USA).

3. Results and discussions

3.1. Fabrication and characterization of GFLC

Considering the advantages of modularization for electrochemical biosensor, we have fabricated GFLC as a module with multi-functions including molecular recognition, signal amplification and output. As shown in Fig. 1(A), electroactive probe Fc and recognition unit hydrazine can be simultaneously self-assembled onto the surface of FTL. AuNPs with signal amplification effect can be chemoselectively linked to liposome through hydrazone chemistry, resulting in the formation of GFLC.

We have verified the formation of GFLC through the combination of different techniques. As shown in Fig. 1(B), AuNPs-Cys-GAP shows the typically spherical shape (Image a) and the synthesized FTL nanoparticles maintained their spherical shape with clear thin shell without any rupture, suggesting the formation of a typical vesicle structure (Zhao et al., 2017) (Image b). Moreover, a three dimensional cluster can be observed for GFLC (Image c, Fig. 1(B)). The cluster is constructed through the linkage of AuNPs-Cys-GAP with FTL via hydrazone chemistry. A new absorption peak at 1627 cm^{-1} which can be attributed to stretching vibration of C=N, can be found for GFLC (curve b, Fig. 1(D)), in comparison with that of AuNPs-Cys-GAP (curve a, Fig. 1(D)). It well suggests the formation of hydrazone bond for the fabrication of GFLC. Moreover, AFM images clearly illustrate that FTL are well-dispersed on the mica surface with well-defined spherical structures and mean diameters of 200 nm (Image b, Fig. 1(C)). GFLC are aggregated cluster consisted of massive spheres with different sizes (Image c, Fig. 1(C)). Meanwhile, GFLC exhibits a reduced surface charge zeta-potential (-23.5 ± 0.38 mV) compared with that of FTL (-22.3 ± 0.80 mV), resulting from incorporation of negatively charged AuNPs-Cys-GAP (Fig. S2). Furthermore, we further validate the successful fabrication of FTL and GFLC through fluorescence image and fluorescent spectra measurement. As a long-chain carbocyanine dye, Dio is essentially insoluble in water and becomes inserted into the lipid bilayer with its alkyl chains and is widely used for the characterization of membranes (Honig and Hume, 1989). Brightly green fluorescence (Image a, Fig. 1(E)) and an evident emission peak (curve a, Fig. 1(E)) can be observed for FTL, confirming the existence of lipid bilayer. However, almost no fluorescence (Image b, Fig. 1(E)) and a negative peak can be found for GFLC, which can be explained for quench effect of AuNPs on fluorescence of Dio.

3.2. Modularization effect of three-dimensional GFLC for electrochemical biosensor

The performance of GFLC as a module for construction of electrochemical biosensor has been described in Fig. 2(A). Multi-functional GFLC can be linked onto the modified electrode surface through hydrazone bond originating from the reaction between hydrazine groups at the outer layer of GFLC and aldehyde groups of oxidized LPS. Except for molecular recognition function, GFLC plays the key roles of signal output and signal amplification. On the one hand, signal probe Fc can be self-assembled numerously due to large surface of nanoliposome. On the other hand, the abundant AuNPs as bridges, can chemoselectively link with GFLC together to strengthen electron transfer.

In order to confirm modularization function of GFLC, electrochemical experiments have been conducted and the corresponding results have been exhibited in Fig. 2(B) and (C). A significantly increased current value can be observed for GFLC in comparison with those for Fc and FTL, which can be ascribed to occurrence of tremendous signal probes and good conductivity of massive AuNPs. It suggests that GFLC has multi-functions including simultaneous molecular recognition, signal output and amplification. Meanwhile, the lower resistance can be found for GFLC/LPS/PBA/GE compared with that for FTL/LPS/PBA/GE, and the result also well confirms that the enrichment of AuNPs accelerates electron transfer from solution to electrode surface.

3.3. Mechanism investigation for the assay of LPS

The mechanism for electrochemical analysis of LPS is illustrated in Fig. 3(A). GalO can specifically catalyze the oxidation of 6′-OH of Gal residue in LPS into the corresponding aldehyde group, resulting in the formation of product, oxidized LPS. For one thing, oxidized LPS containing numerous dihydroxyl groups positioned in the cis-form, can coordinate with the boronic acid group of PBA to generate membered ring esters, thus triggering the capture of target by PBA/GE under acidic condition. Our previous experiment has approved that LPS can specially bind with aminophenylboronic acid modified assembled magnetic nanospheres at acidic pH (Li et al., 2017). For another, oxidized LPS with massive aldehyde groups can react with hydrazine groups exposed at the surface of GFLC to form oxime, resulting in occurrence of GFLC on the surface of modified electrode and output of highly sensitive signal. On contrary, there is no formation of oxidized LPS in absence of LPS, thereby GFLC can not be linked onto the surface of PBA/GE and a negligible current value can be obtained. Therefore, LPS amount determines the number of GFLC immobilized onto modified electrode surface, and a new electrochemical method by using GFLC as a module, can be developed.

As shown in Fig. 3(B), a negligible signal peak can be found without LPS (curve a), owing to almost no happening of GFLC on the electrode surface. Inversely, an evident electrochemical signal can be given with LPS (curve b). It well confirms the linkage of GFLC onto the modified electrode surface with the formation of hydrazone bonds. Meanwhile, the appearance of the noticeable peak current can be explained for enrichment of numerous signal probe Fc and favorable electron transfer capability of tremendous AuNPs in GFLC, which has been verified in Fig. 2(B) and (C).

3.4. Specificity investigation for LPS assay

For the investigation of specificity of the established method, different samples including protein (BSA), glycoprotein (Ova and ALP), and substances containing dihydroxyl groups (dopamine and ATP), are

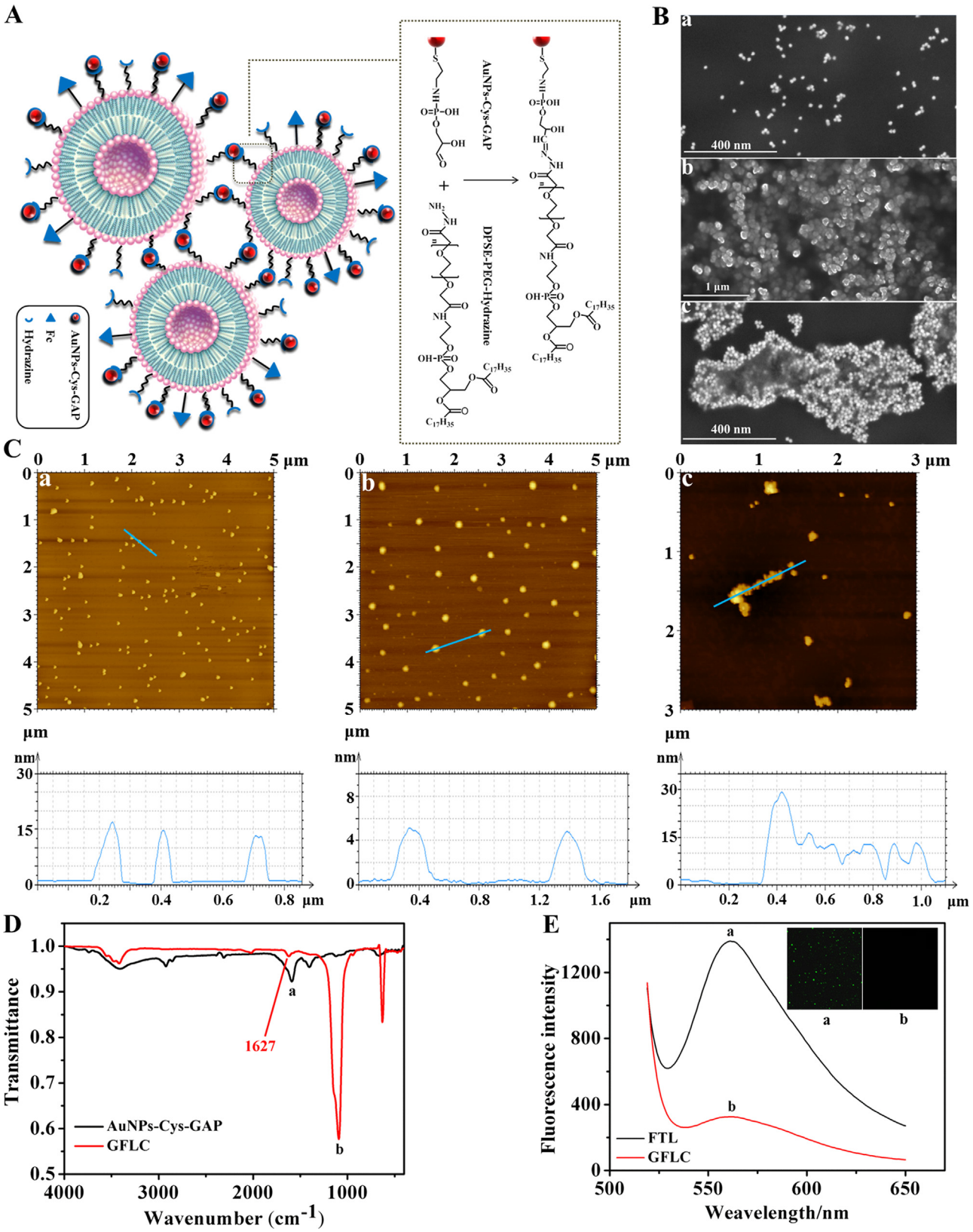

Fig. 1. (A) Schematic illustration for fabrication of GFLC. (B) SEM images and (C) AFM images of (a) AuNPs-Cys-GAP, (b) FTL, and (c) GFLC. (D) FT-IR spectra of (a) AuNPs-Cys-GAP and (b) GFLC. (E) Fluorescence spectra and (Inset) fluorescence images of (a) FTL and (b) GFLC using Dio as molecular probe.

used instead of LPS, and the corresponding results are given in Fig. 4. Except for LPS, other substance can not render the evident increase of current values as a result of nearly no occurrence of GFLC on the surface of electrode. Inversely, high current value can be observed in the presence of LPS, resulting from the formation of boronate ester under acidic condition and subsequent immobilization of GFLC on the surface of modified electrode through hydrazone chemistry.

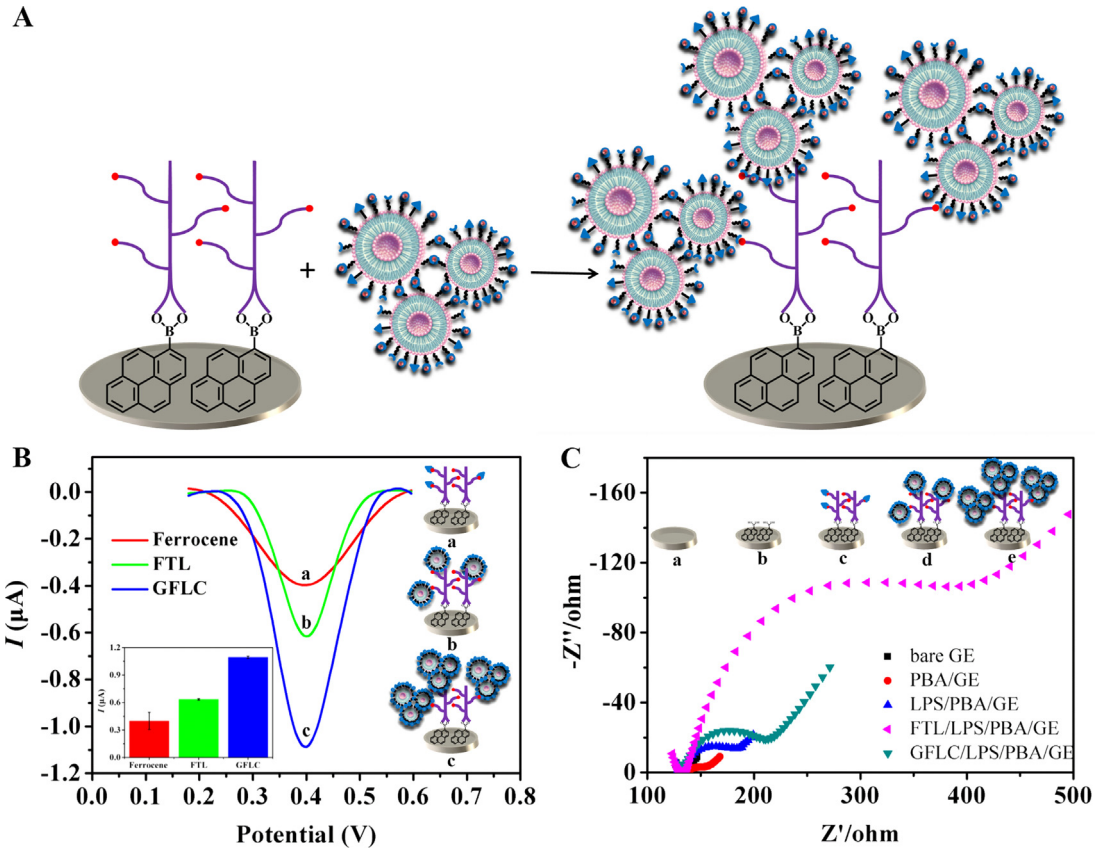

Fig. 2. (A) Schematic illustration for modularization effect of GFLC for construction of electrochemical biosensor. (B) Differential pulse voltammograms and (Inset) peak current for electrochemical biosensor constructed by using Fc, FTL, and GFLC, respectively. The scan rate was 100 mV/s. Inset: schematic illustration for electrochemical biosensor with Fc, FTL, and GFLC, respectively. (C) Complex plane plot for the electrochemical impedance measurements of the graphite electrode at different modification stages: (a) bare GE, (b) PBA/GE, (c) LPS/PBA/GE, (d) FTL/LPS/PBA/GE, and (e) GFLC/LPS/PBA/GE. Electrochemical species: 5 mM $[Fe(CN)_6]^{3-/4-}$ containing 0.1 M KCl, Electrolyte: 0.01 M $NaClO_4$ (pH = 7.0), Biasing potential: 0.224 V, Amplitude: 5 mV, and Frequency range: 0.01 Hz - 10 kHz. Inset: schematic illustration for the graphite electrode at different modification stages.

3.5. Electrochemical assay of LPS

Differential pulse voltammograms upon analyzing different amounts of LPS are shown in Fig. 5(A). With the increase of LPS concentrations from 0 μg/mL to 8 μg/mL, the peak current values gradually rise. It implies the increasing loading of GFLC onto the surface of electrode. Boronic acid groups exposed on the electrode surface, can specifically capture LPS at acidic pH values, followed by the immobilization of GFLC due to the occurrence of aldehyde groups on the surface of modified electrode after the binding of LPS. Hence the increasing amount of LPS can result in corresponding increasing binding of GFLC onto the electrode surface.

The peak current values have been further used to quantitatively detect LPS and the corresponding results are shown in Fig. 5(B). The current values linearly increase with logarithmic values of increasing enzyme concentrations from 2×10^{-9} μg/mL to 8 μg/mL, which is wider than previous reports (Bai et al., 2014; Cho et al., 2012; Lan et al., 2012; Li et al., 2017; Shen et al., 2015; Voss et al., 2007; Xie et al., 2016a, 2016b; Zeng et al., 2010). The linear fitting equation of $I = 1.07077 + 0.03468 \lg C_{LPS}$ (μg/mL) can be obtained with a

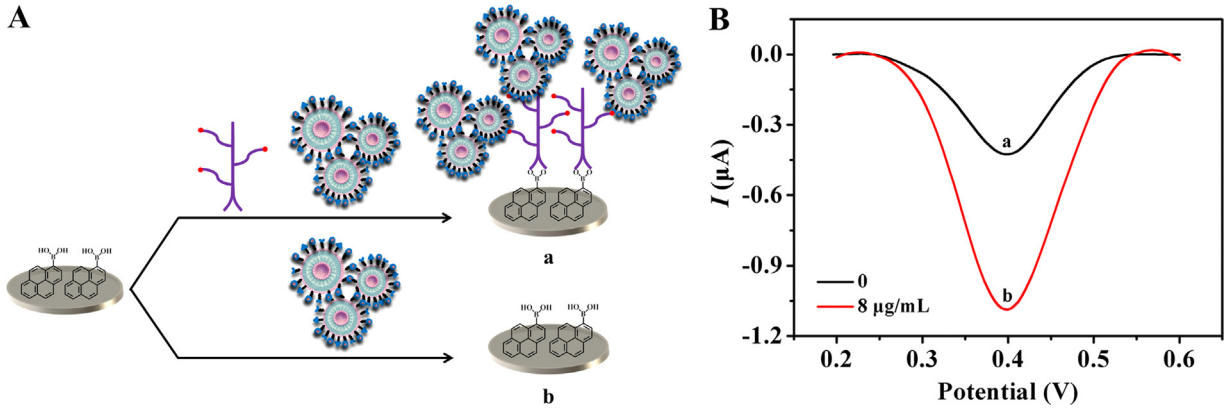

Fig. 3. (A) Schematic illustration of mechanism for electrochemical analysis of LPS by using GFLC. (B) Differential pulse voltammograms with different LPS concentrations at (a) 0 and (b) 8 μg/mL. Scanning rate: 100 mV/s. Different columns with different letters are significantly different ($p \leq 0.05$).

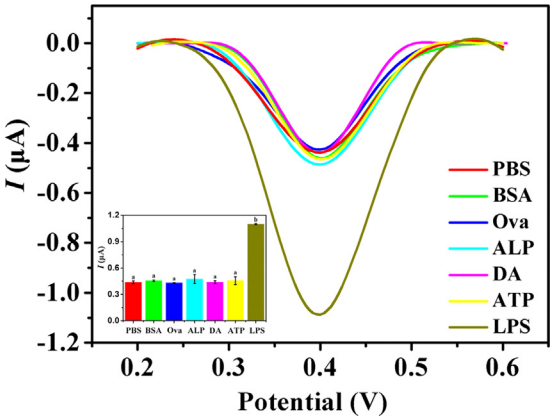

Fig. 4. Differential pulse voltammograms and (Inset) peak current values for the specificity investigation of the established electrochemical method against the different samples: Blank, BSA (8 μg/mL), Ova (8 μg/mL), ALP (8 μg/mL), DA (8 μg/mL), ATP (8 μg/mL), and LPS (8 μg/mL). Error bars are obtained based on three independent measurements. Different columns with different letters are significantly different ($p \leq 0.05$).

correlation coefficient of $R^2 = 0.99901$, where I is the peak current value and C_{LPS} is LPS concentration. The detection limit is estimated to be 0.51×10^{-10} μg/mL (3 times signal to noise ratio), which is lower than the values in the previous report (Bai et al., 2014; Cho et al., 2012; Lan et al., 2012; Li et al., 2017; Shen et al., 2015; Voss et al., 2007; Xie et al., 2016a, 2016b; Zeng et al., 2010). Meanwhile, the electrochemical experiments have been conducted three times and a 3.4% of RSD value has been obtained by using the slopes of three regression equations with LPS concentrations from 2×10^{-9} μg/mL to 8 μg/mL. It signifies acceptable reproducibility and precision of the developed electrochemical method.

3.6. LPS assay in the soft drinks samples

In order to evaluate the practicable application of the established electrochemical biosensor, a certain amount of LPS is added into different soft drinks and the LPS concentrations are determined using our established method (Table 1). The recovery ratio varies from 90% to 110% and the RSD values are basically within 5%. These results indicate that our method owns good anti-interfering capability and can well serve for LPS analysis in the real samples.

Table 1
LPS concentrations detected by our method and the comparison with the given concentrations in soft drinks samples.

Sample	LPS concentration detected(mg/mL)	Standard concentration (mg/mL)	Relative error (%)	Relative error (%)
Purifiedwater	1.9724	2	98.62	3.1
	8.1846×10^{-3}	8×10^{-3}	102.31	4.9
	2.1188×10^{-6}	2×10^{-6}	105.94	2.5
	7.7037×10^{-9}	8×10^{-9}	96.3	1.7
Milk	1.8454	2	92.27	4.7
	7.9744×10^{-3}	8×10^{-3}	99.68	1.5
	2.0893×10^{-6}	2×10^{-6}	104.47	3.4
	7.9104×10^{-9}	8×10^{-9}	98.88	2.7
Grapefruit juice	2.1077	2	105.38	3.1
	7.7144×10^{-3}	8×10^{-3}	96.43	2
	1.9697×10^{-6}	2×10^{-6}	98.49	1.3
	8.2871×10^{-9}	8×10^{-9}	103.59	2.3
Green Tea	1.8454	2	92.27	4.1
	8.4645×10^{-3}	8×10^{-3}	105.8	3.5
	2.1473×10^{-6}	2×10^{-6}	107.37	2.1
	7.5509×10^{-9}	8×10^{-9}	94.39	4.8

4. Conclusions

In conclusion, GFLC has been designed and fabricated as a module for construction of electrochemical biosensor. With numerous hydrazine groups, massive electrochemical probe Fc, and tremendous AuNPs, GFLC plays three roles including molecular recognition, signal output and amplification. With multi-functionality, GFLC has been successfully applied for electrochemical detection of LPS in various food samples. The relatively low detection limit of 0.51×10^{-10} μg/mL can be obtained with a wide linear range from 2×10^{-9} μg/mL to 8 μg/mL. In view of these advantages of GFLC as a module, we anticipate that the multi-functionalized design strategy will provide a new sight for the establishment of electrochemical biosensors and well serve for the development of biosensor.

Acknowledgement

This work is supported by the National Natural Science Foundation of China (Grant nos. 31671923, 81503463, and 31571763) and Shanghai Pujiang Program (Grant no. 18PJD016).

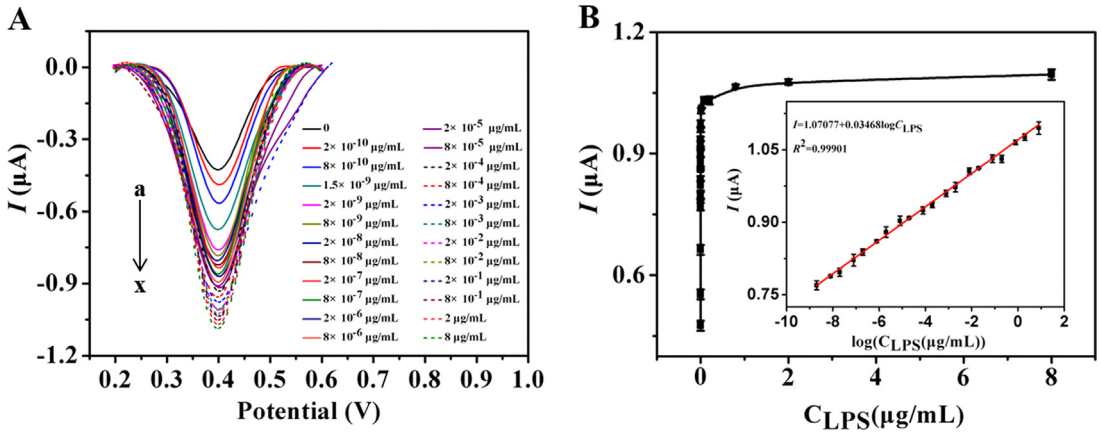

Fig. 5. (A) Differential pulse voltammograms for LPS at different concentrations: (a) 0, (b) 2×10^{-10}, (c) 8×10^{-10}, (d) 1.5×10^{-9}, (e) 2×10^{-9}, (f) 8×10^{-9}, (g) 2×10^{-8}, (h) 8×10^{-8}, (i) 2×10^{-7}, (j) 8×10^{-7}, (k) 2×10^{-6}, (l) 8×10^{-6}, (m) 2×10^{-5}, (n) 8×10^{-5}, (o) 2×10^{-4}, (p) 8×10^{-4}, (q) 2×10^{-3}, (r) 8×10^{-3}, (s) 2×10^{-2}, (t) 8×10^{-2}, (u) 2×10^{-1}, (v) 8×10^{-1}, (w) 2 and (x) 8 μg/mL. (B) Peak current values versus different concentrations of LPS. Inset: The linear relationship between peak current values and the logarithmic values of LPS concentrations.

Appendix A. Supporting information

Supplementary data associated with this article can be found in the online version at doi:10.1016/j.bios.2018.09.101.

References

Bai, L., Chai, Y., Pu, X., Yuan, R., 2014. A signal-on electrochemical aptasensor for ultrasensitive detection of endotoxin using three-way DNA junction-aided enzymatic recycling and graphene nanohybrid for amplification. Nanoscale 6 (5), 2902–2908.

Beutler, B., Rietschel, E.T., 2003. Innate immune sensing and its roots: the story of endotoxin. Nat. Rev. Immunol. 3 (2), 169–176.

Bui, M.P., Ahmed, S., Abbas, A., 2015. Single-digit pathogen and attomolar detection with the naked eye using liposome-amplified plasmonic immunoassay. Nano Lett. 15 (9), 6239–6246.

Chen, M., Wang, Y., Su, H., Mao, L., Jiang, X., Zhang, T., Dai, X., 2018. Three-dimensional electrochemical DNA biosensor based on 3D graphene-Ag nanoparticles for sensitive detection of CYFRA21-1 in non-small cell lung cancer. Sens. Actuators B: Chem. 255, 2910–2918.

Cho, M., Chun, L., Lin, M., Choe, W., Nam, J., Lee, Y., 2012. Sensitive electrochemical sensor for detection of lipopolysaccharide on metal complex immobilized gold electrode. Sens. Actuators B: Chem. 174, 490–494.

Deng, H.H., Wu, C.L., Liu, A.L., Li, G.W., Chen, W., Lin, X.H., 2014. Colorimetric sensor for thiocyanate based on anti-aggregation of citrate-capped gold nanoparticles. Sens. Actuators B: Chem. 191, 479–484.

Honig, M.G., Hume, R.I., 1989. Dil and DiO: versatile fluorescent dyes for neuronal labelling and pathway tracing. Trends Neurosci. 12 (9), 333–341.

Jia, H., Xu, J., Lu, L., Yu, Y., Zuo, Y., Tian, Q., Li, P., 2018. Three-dimensional Au nanoparticles/nano-poly(3,4-ethylene dioxythiophene)- graphene aerogel nanocomposite: a high-performance electrochemical immunosensing platform for prostate specific antigen detection. Sens. Actuators B: Chem. 260, 990–997.

Kumarasamy, J., Camarada, M.B., Venkatraman, D., Ju, H., Dey, R.S., Wen, Y., 2018. One-step coelectrodeposition-assisted layer-by-layer assembly of gold nanoparticles and reduced graphene oxide and its self-healing three-dimensional nanohybrid for an ultrasensitive DNA sensor. Nanoscale 10 (3), 1196–1206.

Lan, M., Wu, J., Liu, W., Zhang, W., Ge, J., Zhang, H., Sun, J., Zhao, W., Wang, P., 2012. Copolythiophene-derived colorimetric and fluorometric sensor for visually supersensitive determination of lipopolysaccharide. J. Am. Chem. Soc. 134 (15), 6685–6694.

Lee, J., Kim, H.J., Kim, J., 2008. Polydiacetylene liposome arrays for selective potassium detection. J. Am. Chem. Soc. 130 (15), 5010–5011.

Lei, J., Ju, H., 2012. Signal amplification using functional nanomaterials for biosensing. Chem. Soc. Rev. 41 (6), 2122–2134.

Li, D., Sun, T., Zhang, W., Shen, Z., Zhang, J., 2017. Colorimetric analysis of lipopolysaccharides based on its self-assembly to inhibit ion transport. Anal. Chim. Acta 992, 85–93.

Luo, X., Morrin, A., Killard, A.J., Smyth, M.R., 2006. Application of nanoparticles in electrochemical sensors and biosensors. Electroanalysis 18 (4), 319–326.

Murai, T., Ogawa, Y., Kawasaki, H., Kanoh, S., 1987. Physiology of the potentiation of lethal endotoxin shock by streptococcal pyrogenic exotoxin in rabbits. Infect. Immun. 55 (10), 2456–2460.

Nie, J., Zhang, D.W., Tie, C., Zhou, Y.L., Zhang, X.X., 2013. A label-free DNA hairpin biosensor for colorimetric detection of target with suitable functional DNA partners. Biosens. Bioelectron. 49, 236–242.

Prakash, S., Chakrabarty, T., Singh, A.K., Shahi, V.K., 2013. Polymer thin films embedded with metal nanoparticles for electrochemical biosensors applications. Biosens. Bioelectron. 41, 43–53.

Qian, R., Cao, Y., Long, Y.T., 2016. Dual-targeting nanovesicles for in situ intracellular imaging of and discrimination between wild-type and mutant p53. Angew. Chem. Int. Ed. 55 (2), 719–723.

Shen, W.J., Zhuo, Y., Chai, Y.Q., Yuan, R., 2015. Cu-based metal-organic frameworks as a catalyst to construct a ratiometric electrochemical aptasensor for sensitive lipopolysaccharide detection. Anal. Chem. 87 (22), 11345–11352.

Sun, Y., Hong, S., Xie, R., Huang, R., Lei, R., Cheng, B., Sun, D.E., Du, Y., Nycholat, C.M., Paulson, J.C., Chen, X., 2018. Mechanistic investigation and multiplexing of liposome-assisted metabolic glycan labeling. J. Am. Chem. Soc. 140 (10), 3592–3602.

Tian, Y., Tetsu, T., 2005. Mechanisms and applications of plasmon-induced charge separation at TiO2 films loaded with gold nanoparticles. J. Am. Chem. Soc. 127 (20), 7632–7637.

Voss, S., Fischer, R., Jung, G., Wiesmuller, K.H., Brock, R., 2007. A fluorescence-based synthetic LPS sensor. J. Am. Chem. Soc. 129 (3), 554–561.

Wang, F., Hu, S., 2009. Electrochemical sensors based on metal and semiconductor nanoparticles. Microchim. Acta 165 (1–2), 1–22.

Xie, P., Zhu, L., Shao, X., Huang, K., Tian, J., Xu, W., 2016a. Highly sensitive detection of lipopolysaccharides using an aptasensor based on hybridization chain reaction. Sci. Rep. 6, 29524.

Xie, S., Dong, Y., Yuan, Y., Chai, Y., Yuan, R., 2016b. Ultrasensitive lipopolysaccharides detection based on doxorubicin conjugated n-(aminobutyl)-n-(ethylisoluminol) as electrochemiluminescence indicator and self-assembled tetrahedron dna dendrimers as nanocarriers. Anal. Chem. 88 (10), 5218–5224.

Yang, R.B., Mark, M.R., Gray, A., Huang, A., Xie, M.H., Zhang, M., Goddard, A., Wood, W.I., Gurney, A.L., Godowski, P.J., 1998. Toll-like receptor-2 mediates lipopolysaccharide-induced cellular signalling. Nature 395 (6699), 284–288.

Yuan, C.X., Fan, Y.R., Tao, Z., Guo, H.X., Zhang, J.X., Wang, Y.L., Shan, D.L., Lu, X.Q., 2014. A new electrochemical sensor of nitro aromatic compound based on three-dimensional porous Pt–Pd nanoparticles supported by graphene–multiwalled carbon nanotube composite. Biosens. Bioelectron. 58, 85–91.

Zeng, L., Wu, J., Dai, Q., Liu, W., Wang, P., Lee, C.S., 2010. Sensing of bacterial endotoxin in aqueous solution by supramolecular assembly of pyrene derivative. Org. Lett. 12 (18), 4014–4017.

Zhang, D.W., Nie, J., Zhang, F.T., Xu, L., Zhou, Y.L., Zhang, X.X., 2013. Novel homogeneous label-free electrochemical aptasensor based on functional DNA hairpin for target detection. Anal. Chem. 85 (19), 9378–9382.

Zhang, Y., Xue, Q., Liu, J., Wang, H., 2017. Magnetic bead-liposome hybrids enable sensitive and portable detection of DNA methyltransferase activity using personal glucose meter. Biosens. Bioelectron. 87, 537–544.

Zhao, Y., Chen, X., Lin, S., Du, D., Lin, Y., 2017. Integrated immunochromatographic strip with glucometer readout for rapid quantification of phosphorylated proteins. Analtica Chim. Acta 964, 1–6.

Zhou, J., Wang, Q.X., Zhang, C.Y., 2013. Liposome–quantum dot complexes enable multiplexed detection of attomolar dnas without target amplification. J. Am. Chem. Soc. 135 (6), 2056–2059.